OPTIMIZATION OF JOINT SAND BARRIER SPACING AND CHARACTERIZATION OF WIND AND SAND FLOW STUDY BASED ON CFD NUMERICAL SIMULATION
/
基于CFD 数值模拟的联合沙障间距优化与风沙流特征研究

Ming YAN[1]; Afang JIN *[1]; Wenxiu GAO [1]
[1] College of Mechanical Engineering, Xinjiang University, Urumqi 830046/ China;
Tel: +86-18999869949; E-mail: jinaf3500_xju@xju.edu.cn
DOI: https://doi.org/10.35633/inmateh-73-72

Keywords: *Agricultural security, numerical simulation, wind tunnel experiment, wind sand, combined sand barrier, optimal spacing*

ABSTRACT
Strong wind and sand activities will seriously damage the ecological restoration and agricultural safety production on the edge of desert areas, resulting in irreversible economic losses. To prevent and protect the agroecological environment in the wind-blown sand area, this paper constructs a combination of double-row vertical nylon net sand barrier and grass grid sand barrier. The protection benefits of double-row vertical nylon net sand barrier and grass grid under different spacing conditions are analyzed through numerical simulation and wind tunnel experiment, and the layout conditions with optimal spacing are obtained. The results show that when the spacing between the double-row vertical sand barrier and grass grid is 5H-10H, the airflow velocity behind the double-row vertical sand barrier cannot be fully developed, the increase of airflow velocity is small, and the average wind prevention efficiency is above 85%. The effective protection distance completely covers the entire combined sand barrier area, and a large number of sand particles near the surface are fixed to the grass grid, so the sand resistance rate is over 77%. The combined sand barrier has a good cooperative protection effect and achieves efficient wind prevention and sand fixation. The wind tunnel experiment verifies the reliability of the results. It also realizes efficient wind prevention and sand fixation under extreme wind and sand, and avoids sand burial on farmland and ecological restoration areas caused by extreme wind and sand weather.

摘要
强烈的风沙活动会对沙漠地区边缘地带的生态恢复建设和农业安全生产形成严重破坏，造成不可逆转的经济损失。为预防保护风沙地区的农业生态环境，本文构建了双排高立式尼龙网沙障＋草方格联合沙障，通过数值模拟和风洞实验，分析双排高立式尼龙网沙障与草方格不同间距条件下的防护效益，得到了最优间距的布设工况。结果表明，当双排高立式沙障与草方格间距为 5H-10H 时，双排高立式沙障后气流速度无法充分发育，气流速度增大幅度较小，平均防风效率达到 85％以上，有效防护距离完全覆盖整个联合沙障区域，近地表沙粒大量被固定至草方格内，阻沙率达到 77％以上，联合沙障协同防护作用较好，实现高效的防风固沙。经风洞实验测试，验证了结果的可靠性。实现了在极端风沙天气下高效的防风固沙，避免极端风沙天气对农田和生态修复区造成沙埋。

INTRODUCTION
China has most extensive desert distribution in the world, mainly concentrated in Xinjiang, Gansu, Inner Mongolia, and Qinghai *(Xiao J., 2016)*. Wherever the strong air currents carrying sand particles pass, large areas of farmland are buried by sand or blown away by wind erosion through sand burial, wind erosion, and wind attacks, resulting in the deterioration of the ecological environment and severe losses to people's lives and property *(Zhenghua Z., 2006; Ming W., 2007)*.

Protective measures are divided into sand-blocking and sand-fixing measures to protect the ecological restoration area around the desert plants and farmland from sandstorms, generally in the oasis edge of the deployment of protective measures. Mechanical sand barriers have the advantages of anti-aging, anti-wind-sand, industrial production, convenient construction, in some fields with serious wind-sand disasters, such as industry and mining, transportation and national defense, the use of mechanical sand barriers can achieve rapid results *(Maolin W., Ling S. et al., 2024)*.

Ming Yan, M.S.Stud; Afang Jin, Professor; WenXiu Gao, M.S. Stud

Among the sand-fixing sand barriers, the most typical one is the grass grid sand barrier. Grass grid plays an irreplaceable role in wind prevention and sand fixation, precipitation interception, water evaporation reduction and nutrition for sand and soil *(Jiayuan D, Xiangyun Q, 2019)*. One of the direct functions of grass grid sand barrier is to increase the surface aerodynamic roughness Z_0, the aerodynamic roughness of Z_0 is hundreds to thousands of times larger than the surface of quicksand, thus significantly reducing the ground surface wind speed, making it lower than the sand generating wind speed, and maintaining the stability of the sand surface in the grid *(Junling X., 1982; Yingxin L., 1987; Jiguo Z., 1987; Dong, Chen et al., 2002)*. Another direct effect is to physically block the aeolian sand flow and promote the rapid settlement of the transit aeolian sand flow *(Congmao K., 2000; Yizheng Y., Guanging C. et al., 2006; Guoping Z., Hejun Z. et al., 2008)*.

Qu Jianjun *(Jianjun Q., 2001; Jianjun Q., 2002)* conducted wind tunnel simulation experiments on the effect of nylon mesh sand prevention, and found that nylon mesh sand barrier fence is more efficient than wooden sand barrier fence, which is a high-quality new material for sand prevention. The results show that the double row of wind grids is the best through numerical simulation and wind tunnel tests, combined with economy and effective shielding distance *(Fang, Wu et al., 2018)*. *Dong, Chen et al., (2023),* pointed out that double-row and three-row wind fences are the most effective in reducing wind speed, which was confirmed in subsequent studies (*Cornelis and Gabriels, 2004*). For the line spacing, *Papesch, (1992),* and *Wu, Zou et al., (2013),* recommended 6-8 H (H is the height of the wind fence) as being the best.

Guangpu J., Hejun Z. et al., (2020), showed in the experiment that the distance between the double-row sand barriers at the height of 150 cm was 20 m when the wind speed increased to more than 15 m/s, there was basically no sand accumulation on the lee side of the double-row sand barriers, and the high-vertical sand barriers gradually lost their protective effect. There is a certain relationship between the height of sand barriers and the protection distance. *Wang Xunming et al. (1997; 1999),* found in the analysis of the benefits of the Tarim Desert highway sand prevention system that laying vertical nylon net sand barriers with a height of 1.1 m on flat sandy land can achieve a protection range of about 10 m. Xu et al. 's numerical simulation analysis found that there were a series of non-uniformly distributed eddies in the grass grid, which would carry sand particles near the grass belt and accumulate them, promoting the formation of concave surfaces *(Xu, Zhang et al., 2018)*. Based on the aerodynamic principle of sand movement, Wang Zhenting *(Zhenting W., 2002)* obtained the analytical formula for the optimal correlation between the surface height of wheat grass and the side length of the grid by using numerical simulation. *Qiu, Lee et al., (2004),* used a computational fluid dynamics (CFD) model to simulate the wind speed profiles of wheat grass sand barriers of different specifications. Considering the cost and protection benefits comprehensively, it is suggested to set the sand barriers with a specification of 1m×1m and a height of 10-20 cm. *Zhang, Li et al., (2016),* observed the wind speed and sand transport rate of bare sand. They paved grass square sand barriers through field comparison, and found that the height of 20 cm sand barriers can improve the surface roughness by more than 0.02 m, and the sand transport rate above the sand barriers changes with the height of the contour in the form of a weevil.

The combined sand barrier and grass grid have the function of blocking solid combination, which can produce better protective efficiency. Through wind tunnel experiment and numerical simulation, *Xin, Zhang et al., (2023),* studied the optimal porosity and opening type of the second sand barrier in the combination of double-row nylon mesh high vertical sand barrier and grass grid sand barrier, and found that when the second high vertical sand barrier had a horizontal opening, the second high vertical sand barrier destroyed the continuous flow of particles from the first sand fence. Thus, most of the sand is deposited on the leeward side and in the grass grid, improving the wind and sand prevention efficiency. *Peng, Jin et al., (2023),* used the computational fluid dynamics method and the Eulerian-Eulerian two-fluid model to simulate the wind protection effect and the airflow characteristics of the newly developed double-row reed-nylon mesh combination sand barrier, which is made of different materials, and combines the advantages of both, improving the construction efficiency and service life for deserts. It also provides a more economical and efficient reference for the layout of windscreen sand facilities around railways and highways in desert areas.

To sum up, domestic and foreign scholars have a large research foundation for the study of wind and sand resistance performance and mechanism of single sand barrier and sand-fixation barrier. It also has accumulated profound experience in the application of various technical means in continuous in-depth research. However, the effect of combined sand barrier and how it can be used it in engineering measures are still mainly based on engineering experience. So, there is a lack of systematic experimental and theoretical research and few studies on the protection ability of the protection system under extreme wind and sand environment. To avoid destroying ecological restoration areas and farmland economic losses, we study the wind and sand prevention facilities in this kind of extreme weather.

Therefore, this paper takes the combination of double-row high vertical nylon net sand barrier and straw checkerboard barrier as the research object, the numerical simulation as the primary research method, the wind tunnel test as the verification method, the maximum field wind speed as the inlet wind speed condition, studies the protection benefits under the conditions of different spacing between double-row high vertical nylon net sand barrier and grass grid, and obtains the layout conditions with the optimal spacing. It provides a theoretical basis for the design of sand control projects in desertification ecological restoration areas.

MATERIALS AND METHODS

Overview of the study area

Minqin County of China is located in the northeast of Hexi Corridor, the lower reaches of the Shiyang River basin, the south adjacent to Wuwei, southwest adjacent to Jinchang, east, west, north three sides, surrounded by Tengger Desert and Badain Jaran Desert *(Yanli Z., 2011)*. The study area is a temperate continental arid climate, with northwest winds throughout the year, with an average wind ≥12 m/s and the instantaneous wind ≥17 m/s, the gale weather above grade 8 is more frequent, the maximum wind speed is 11, the average gale days in the county are 27.8 days, the maximum is 63 days, the sand storm is 25 days, the sand blowing is 37.5 days, and the sand-driving wind speed is 4.5, the average yearly temperature is 7.7℃, the annual average precipitation is 48-185 mm, and the rainfall is mainly concentrated in July to September. So, the soil desertification phenomenon in the territory is severe, the desert area is vast, the desert vegetation is sparse, the composition types are scarce, and the vegetation structure is simple *(Fugui H., Ming Z. et al., 2009; Cuicui J., Xuemei Y. et al., 2021)*. Minqin Oasis is the front line of desertification resistance in northern China, and an ecological fortress to protect the unimpeded flow of the Eurasian Continental Bridge, which needs effective wind and sand blocking facilities to protect, so it is necessary to rationally configure according to the degree of sand damage in different areas.

a) ***b)***

Fig. 1 – The current situation of farmland around the desert in Minqin County, China

a) The desert invades the farmland; b) the locals erect sand retaining walls.

Numerical simulation

Theoretical governing equation

This paper, uses the Euler two-phase fluid model to study the near-surface aeolian sand movement with different double rows of vertical sand barriers and grass grid spacing. In this model, the gas phase and solid phase are regarded as continuous media that exist together and permeate each other, and the sum of their volume fractions is 1. That's to say: $\alpha_g+\alpha_s=1$. Gas-solid two-phase flow follows mass conservation and momentum conservation equations, respectively, and the governing equations are as follows:

Gas-phase mass conservation equations:

$$\frac{\partial}{\partial t}\left(\alpha_g\rho_g\right)+\nabla\left(\alpha_g\rho_g v_g\right)=0 \tag{1}$$

Sand-phase mass conservation equations:

$$\frac{\partial}{\partial t}\left(\alpha_s\rho_s\right)+\nabla\left(\alpha_s\rho_s v_s\right)=0 \tag{2}$$

The gas-phase momentum conservation equation:

$$\frac{\partial}{\partial t}(\alpha_g\rho_g U_g)+\nabla(\alpha_g\rho_g U_g U_g)=-\alpha_g\nabla p+\nabla\tau_g+\alpha_g\rho_g g+K_{gs}(U_g-U_s) \tag{3}$$

Sand-phase momentum conservation equations:

$$\frac{\partial}{\partial t}(\alpha_s \rho_s U_s) + \nabla(\alpha_s \rho_s U_s U_s) = -\alpha_s \nabla p - \nabla p_s + \nabla \tau_s + \alpha_s \rho_{sg} + K_{sg}(U_s - U_g) \quad (4)$$

Gas-solid interaction forces:

$$f_{sg} = \frac{3\, C_D a_s a_s \rho_g}{4d} |U_r| U_r a_g^{-2.65} \quad (5)$$

In this equation, α_g, α_s are the volume fractions of the gas and sand phases, t is the time, ρ_g, ρ_s are the densities of the gas and sand phases, respectively, v_g, v_s are the velocity vectors of the gas and sand phases, respectively; U_g, U_s, are the velocities of the gas and sand phases, respectively, and τ_g, τ_s are the surface stress tensors of the gas and sand phases, respectively; p is the same pressure shared by the two phases. p_s is the pressure of the sand phase, and g is the acceleration of gravity, so $K_{gs} = K_{sg}$, and they are the momentum exchange coefficients of the gas and solid phases, respectively. C_D is the drag coefficient; U_r is the relative velocity between the gas and solid phases; and d is the diameter of the sand grain.

The standard k-ε turbulence model was used in this study. Air is defined as an incompressible flow without heat exchange. According to the multiphase fluid theory, with the gas phase as the dominant phase, the sand phase as the dilute phase, and the volume fraction of the sand phase as 0.02, the turbulence is considered to be fully developed.

Turbulent kinetic energy equation:

$$\rho \frac{\partial(k)}{\partial t} + \rho u_i \frac{\partial(k)}{\partial x_i} = \frac{\partial}{\partial x_j}\left[\left(\mu + \frac{\mu_t}{\sigma_k}\right)\frac{\partial k}{\partial x_j}\right] + G_k - \rho_\varepsilon \quad (6)$$

Turbulent dissipation rate equation (TDR):

$$\rho \frac{\partial(\varepsilon)}{\partial t} + \rho u_i \frac{\partial(\varepsilon)}{\partial x_i} = \frac{\partial}{\partial x_j}\left[\left(\mu + \frac{\mu_t}{\sigma_\varepsilon}\right)\frac{\partial \varepsilon}{\partial x_j}\right] + C_{1\varepsilon} G_k \frac{\varepsilon}{k} - C_{2\varepsilon}\rho \frac{\varepsilon^2}{k} \quad (7)$$

In this equation, u_i is the velocity component along the i direction; t is time. ρ is the air density. k is the turbulent kinetic energy. ε is the turbulent dissipation rate. μ is the dynamic viscosity. μ_t is the turbulent viscosity. G_k is the turbulent kinetic energy generated by the mean velocity gradient. $\sigma_k, \sigma_\varepsilon$ are the Trump constants corresponding to the turbulent kinetic energy and the dissipation rate, σ_k is 1.0, σ_ε is 1.3, $C_{1\varepsilon}$ and $C_{2\varepsilon}$ are constants, $C_{1\varepsilon}$ is 1.44, $C_{2\varepsilon}$ is 1.92.

Geometric modeling and meshing

This model mainly studies the changes in wind-sand flow in the same horizontal section and vertical section, so a two-dimensional model is adopted to simplify the calculation. The size of the flow field in the calculation domain is set as 100m×15m, the positive direction of the X-axis is the direction of the wind-sand flow, the positive direction of the Y-axis is the direction perpendicular to the ground, and the ground at the entrance is the coordinate O point. The calculation domain of the combined sand barrier is shown in Figure 2. The common double rows of high vertical nylon mesh sand barriers and grass grid sand barriers with a porosity of 30% were taken. Among them, the height of the high vertical nylon net sand barrier is 1.5 m. The grass grid sand barrier is composed of a 1m×1m sand-fixing structure, the overall height of the grass grid sand barrier is 0.2 m, and 10 rows are set up in total. In order to simulate the change characteristics of the concentration of Aeolus sand in the Aeolus grid barrier, the Aeolus grid sand barrier model was added to the Aeolus flow model on a flat bed. Here, the permeability of the Aeolus grid and the influence of flexible materials, such as wheat grass on the wind field or such as swaying or vibration, are not considered and the Aeolus grid sand barrier is treated as a rigid body *(Xianpan X., 2015)*. Therefore, the wind tunnel experiment also uses a rigid plastic grid instead. A double-row vertical sand barrier and grass grid combined sand barrier model with spacing D of 7.5 m (5H), 15 m (10H), 22.5 m (15H), and 30 m (20H) is established under different working conditions.

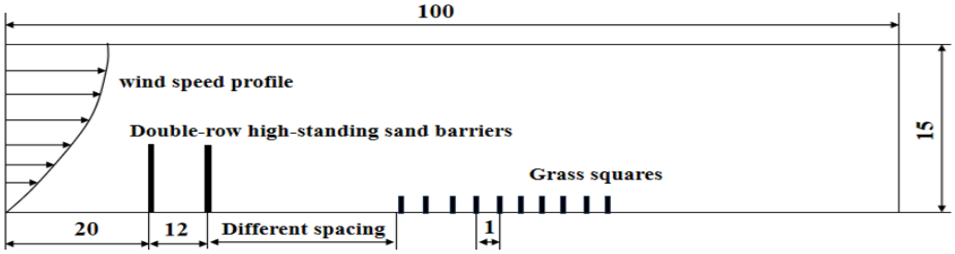

Fig. 2 – Schematic diagram of the computational domain of the joint sand barriers (unit: m)

Considering that the flow field area is large enough, and the influence of the vertical sand barrier on the flow field is mainly the porosity and height, the vertical sand barrier is designed as a wall with no thickness in order to improve the quality of mesh delineation and computational efficiency *(Chang L., Hailong W. et al., 2023)*. The model is meshed by CFD software, the grid type is a Quad (quadrilateral) grid, and the maximum grid size is controlled within 0.2. According to the movement characteristics of wind-blown sand flow, the movement of wind-blown sand flow near the surface is more intense. The grid around the surface and the combined sand barrier is properly encrypted, and 10 boundary layers are set at the bottom, with an increase rate of 1.2. The left and right edges are encrypted at the same time according to the ratio of 1.01, the top is sparse, the bottom is dense, and the total number of grids is about 1.3×10^6.

Boundary condition definition and calculation parameters

The left side of the model is defined as the velocity-inlet, and the wind speed adopts the logarithmic equation of the wind profile. On the right side of the model is a pressure-outlet, with fully developed outflow boundary conditions. The top and sides of the boundary are set as symmetry boundaries, and the ground and sand barriers are defined as non-slip walls. Generally, the particle size carried by the wind-blown sand flow ranges from 0.075 to 0.25 mm. In this paper, the particle size carried by the wind-blown sand flow is 0.1 mm, the sand density is 2600 kg/m^3, and the motion viscosity coefficient of the sand particle is μ= $0.047P_s \cdot s$ *(Guowei, Ning et al., 2021)*. According to statistics, the flow density of wind sand is on the 10^{-5}g·m^{-3} order of magnitude, and the sand phase is sparse, so the initial sand phase volume fraction is 0.02 *(Liangying L., Zhizhong T. et al., 2024)*.

$$V=\frac{V_*}{k}In\frac{y}{z_0} \tag{7}$$

In this equation, V is the horizontal wind speed at y height [m·s^{-1}] and y are the height of the entrance boundary from the bottom surface. And k are the von Karman constants, taking 0.4.V_* is the friction wind speed, [m·s^{-1}] and z_0 is the surface roughness, also the height at which the average wind speed near the ground is 0. Generally, 1/30 of the average particle size of the sand on the bed surface is taken.

Wind tunnel experiment

The wind tunnel test was carried out by the small direct flow wind tunnel experiment platform of Intelligent Manufacturing Modern Industry College of Xinjiang University. It consists of five parts: power section, rectification section, sand supply device, test section and diffusion section. The scale of the model is 1:20. The wind tunnel inlet axis simulation indicates wind speed $v_{\infty_m}=\sqrt{\frac{1}{20}}v_{\infty}=0.224v_{\infty_0}$. v_{∞_0} is prototype indicator wind speed. Considering the wind speed in the field is 30 m·s^{-1}, so the wind speed indicated in this paper is $v_{\infty_m}=$ 7±0.05 m·s^{-1}.

Fig. 3 – Real picture of the wind tunnel

The model was fixed at 1 m away from the sand source, and the inlet wind speed was 7 m/s. Before the experiment, the wind speed at different heights was measured by Pitot tubes. Rough elements are used to generate turbulent boundary layers. In order to ensure a sufficient supply of sand source, the supply length of the sand bed along the flow direction was 0.3 m, and the sand was continuously supplied. The experiment started and continued to blow sand for about 50 minutes. The multi-gradient sand collecting instrument was used to collect sand particles, and the sand collecting instrument was placed 3H behind the combined sand barrier, and the sand accumulation amount under four different spacing distributions was measured respectively. By comparing the sand accumulation amount with that in the open field (same wind speed and sand source, but no wind prevention and sand fixation facilities), the influence of four working conditions on the post-model sand accumulation distribution was studied. The test arrangement is shown in Figure 4.

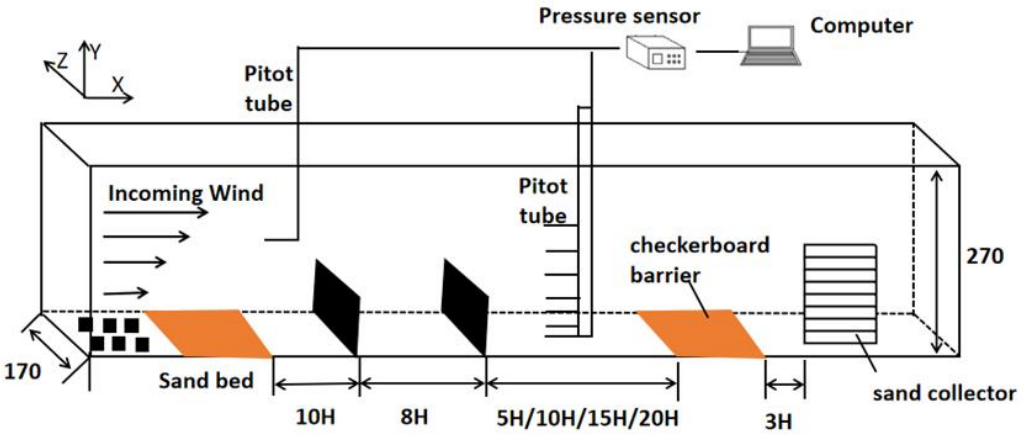

Fig. 4 – Wind tunnel test layout (unit: mm)

Fig. 5 – The layout of wind tunnel experiment

The simulated results of numerical simulation usually need to be verified with wind tunnel tests or field investigations, to ensure the reliability of numerical simulation results. In this paper, the same size model as the wind tunnel test is established for numerical simulation reliability verification under the air field conditions. Based on the solution parameters set in the previous paper, the changes in horizontal wind speed at different heights are simulated and compared with the results of the wind tunnel test.

As shown in Figure. 6, it is found through comparison that the wind speed contour lines of numerical simulation and wind tunnel experiment have good consistency to a certain extent, and there are only some differences at lower heights, but they do not affect the specific calculations. Thus, the parameter selection in this paper is reasonable and accurate, which can provide a precise parameter basis for the subsequent analysis.

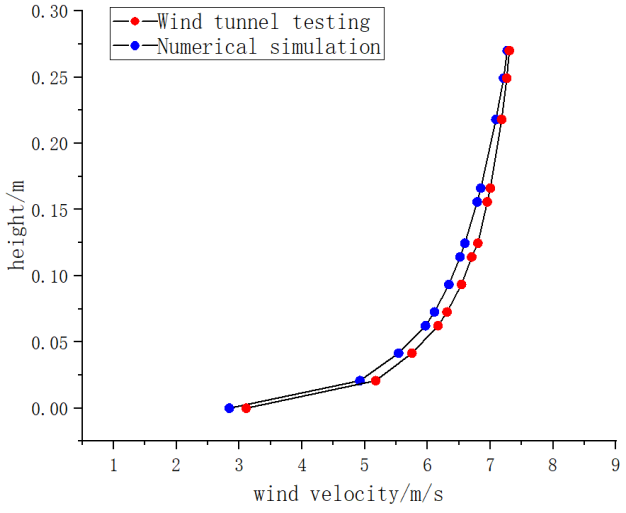

Fig. 6 – Comparison of wind speed profiles from wind tunnel experiments and numerical simulations

RESULTS

Numerical simulation results and analysis

Distribution characteristics of the flow field around the sand barrier

From Figure 7, it can be found that, due to the presence of sand barriers, the airflow deceleration zone is formed on the windward side of the first sand barrier when the wind-driven sand flow enters the flow field, and then most of the airflow rises along the sand barrier to form the airflow acceleration zone. Due to the effect of the sand barrier on airflow collection, the airflow high-speed zone is formed on the sand barrier. The kinetic energy of the other part of the air passing through the pores is reduced, and the direction of the lower part of the air is changed by the action of the mesh plate, forming a large elliptical eddy current region. The distribution characteristics of the flow field around the sand barrier in the four working conditions before the second sand barrier are almost the same, but there is no big difference. The airflow passes through the grass grid sand barrier, forming a low speed-zone in the sand barrier, and finally, the speed gradually recovers at a distance.

Under the four working conditions, due to the different spacing between the high vertical sand barrier and the grass grid barrier, the influence of the low-speed zone behind the second high vertical sand barrier on the grass grid is different. When the spacing is 5H and 10H, the distance between the second vertical sand barrier and the grass grid is relatively close, and a vortex zone of 6 m~8 m is formed between them. The grass grid is basically covered in the low-speed zone, and the wind speed is close to 0, so the sand particles cannot start, and the sand consolidation effect is good. When the spacing is 15H and 20H, the distance between the second vertical sand barrier and the grass grid is far away, and there is a certain range of speed recovery area, the sand is easy to start again, and the grass grid cannot play its sand-fixing role.

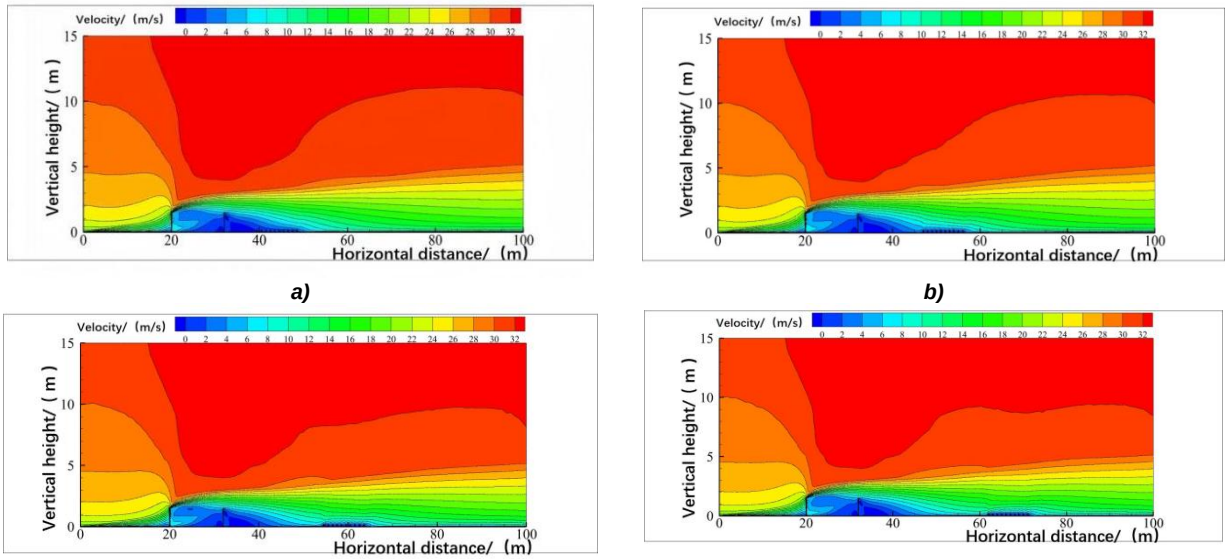

Fig. 7 – Characteristic cloud map of flow field distribution

a) D=5H; b) D=10H; c) D=15H; d) D=20H.

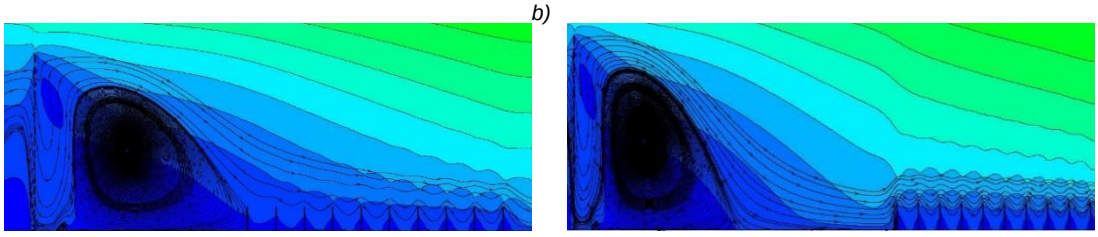

Fig. 8 – Vortex flow diagram

a) D=5H; b) D=10H.

Variation characteristics of horizontal wind speed around sand barriers

The wind-sand flow generally moves close to the surface in the desert, and the near-surface wind speed has a significant effect on the movement of sand particles. Studying the changing trend of air flow around near-surface sand barriers can better analyze the mechanism of sand blocking and fixation *(Zhibao D, 2005)*.

Figure 9 shows the horizontal velocity diagrams around the double-row high vertical nylon mesh sand barriers and grass square joint sand barriers with four spacings at different heights when the inlet velocity is 30 m/s. As can be seen from Figure 9, the sand-carrying wind speed continues to decrease from the entrance, decreases to the minimum value after the second high vertical sand barrier, increases slightly after moving away from the second high vertical sand barrier, and decreases significantly within the height range after encountering the grass grid, and then increases gradually. By comparing the changes in horizontal wind speed under different working conditions, it can be found that within 7 m from the entrance to the second high vertical sand barrier, the change law and amplitude of air velocity are basically the same, and the air velocity is greatly reduced. However, with the increase of spacing, the airflow behind the second vertical sand barrier can fully develop, and the speed increases gradually before reaching the grass grid sand barrier, and the increased amplitude is small in the first and second working conditions. From the third working condition, the increase is obviously greater than the sand-generating wind speed, which is not conducive to the full play of the wind prevention and sand consolidation effect of the grass grid behind. In addition, when the airflow reaches the grass grid, the wind speed is at a small value in the height range, and the wind speed changes less with the increase of the spacing.

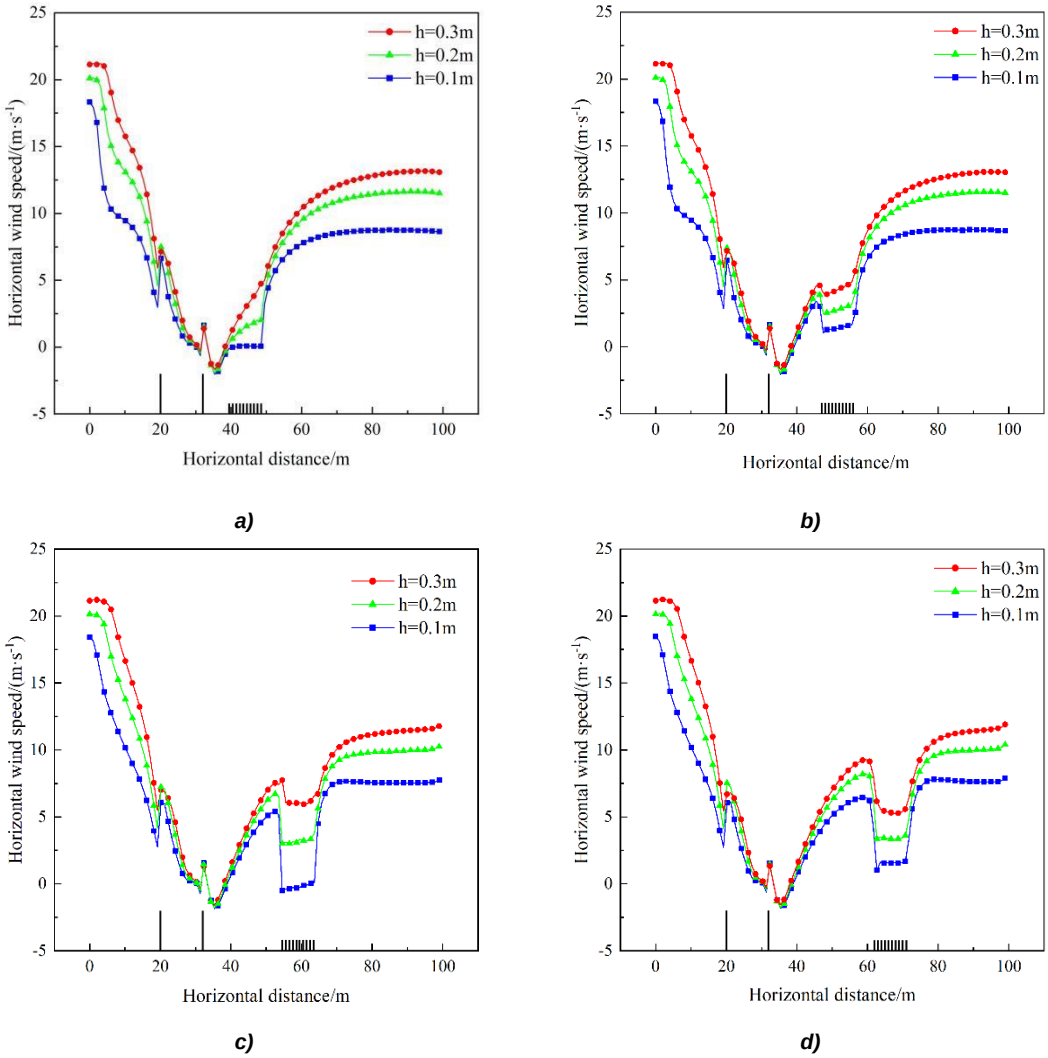

Fig. 9 – Horizontal wind speed map:
a) D=5H; b) D=10H; c) D=15H; d) D=20H.

Windproof efficiency

The wind-proof efficiency of the sand barrier reflects the protective effect of the sand barrier. The greater the wind-proof efficiency, the stronger the block of the sand barrier on the wind sand flow, and the transport of sand particles can be prevented. By extracting the horizontal wind speed at different heights from the flow field, it can be seen that the sand barrier reduces the surrounding wind speed. Therefore, the following formula is used to represent the wind prevention efficiency of the sand barrier *(Tao, Jianjun et al., 2017; Tao, Jianjun et al., 2017):*

$$\Phi_{xy} = \left[1 - \frac{V_{xy}}{V'_{xy}}\right] \times 100\,\% \tag{9}$$

In this equation, Φ_{xy} is the windproof efficiency of the sand barrier, [%]. X is the length from the first sand barrier, [m]. Y is the height from the ground, [m]. When there is sand barrier protection, V_{xy} is the wind speed at point (x, y), [m/s]. When there is no sand barrier protection, V'_{xy} is the wind speed at point (x, y), [m/s].

As shown in Figure 10, when the wind speed from the surface of 0.1 m, 0.2 m, 0.3 m height is taken to calculate the windproof efficiency of the joint sand barriers under different working conditions, it can be found that the closer the windproof efficiency is to the ground, the greater the windproof efficiency is. And it can also be found that the change rule of windproof efficiency at different heights is similar, but there are differences in the windproof efficiency under different working conditions. When the spacing is 5H and 10H, the average windproof efficiency of the combined sand barrier reaches more than 85%, but when the spacing continues to increase, the average windproof efficiency decreases to less than 80%, and the windproof efficiency decreases significantly. When 60% of the wind protection efficiency is taken to determine the effective protection distance, it can be found that the effective protection distance completely covers the entire combined sand barrier area under the conditions of 5H, 10H and 15H, but under the conditions of 20H, the effective protection distance cannot cover the grass grid sand barrier at the height of 0.2 m and 0.3 m.

Table 1

Wind prevention efficiency of combined sand barriers at different spacing

	D=5H	D=10H	D=15H	D=20H
0.1 m	93.28%	90.59%	88.77 %	82.79%
0.2 m	90.24%	87.86%	84.06%	79.12%
0.3 m	87.86%	85.66%	80.29%	76.46%
average	90.46%	88.04%	84.37%	79.45%

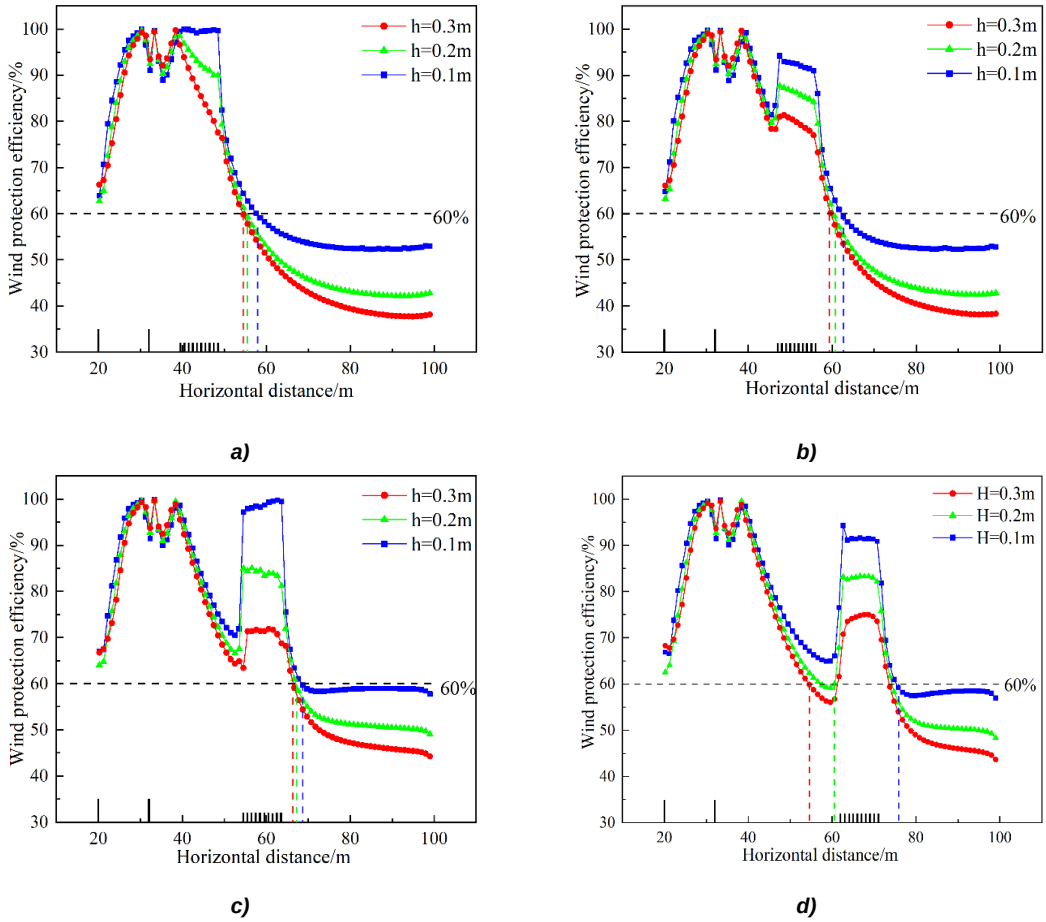

Fig. 10 – Chart of wind protection efficiency and effective protection distance:
a) D=5H; b) D=10H; c) D=15H; d) D=20H.

Location distribution of sediment deposition movement

The mass difference between the airflow and the sand particles is large. When the running wind sand flow encounters obstacles or pressure differences, local resistance will be generated to reduce the wind speed, and at the same time, the energy of the airflow to transport the sand particles will be weakened, causing some sand particles to deposit. The volume distribution of sand particles in the flow field is shown in Figure 11. The larger the volume fraction of sand particles is, the more sand particles are deposited.

It can be found that under different working conditions when the sand-carrying wind passes through the high vertical sand barrier, a large number of sand grains are deposited behind the high vertical sand barrier because the wind speed is greatly reduced to below the sand-generating wind speed. However, due to the different spacing between the grass grid and the high vertical sand barrier, the sand fixation effect of the grass grid is different. Under the conditions of 5H and 10H spacing, due to the close distance between the grass grid and the high vertical sand barrier, there is no space for the wind flow to develop fully after leaving the high vertical sand barrier, and the air flow speed is still low. Coupled with the obstruction effect of the grass grid, a large number of near-surface sand particles are fixed into the grass grid, and the combined sand barrier has a good synergistic protection effect. Under the conditions of 15H and 20H spacing, due to the distance between the grass grid and the high vertical sand barrier, the wind-sand flow can fully recover after leaving the high vertical sand barrier, the airflow speed increases and carries most of the near sand particles up and continues to move backward. So, the sand accumulation in the grass grid is very small, the sand consolidation effect of the grass grid is ineffective, and the synergistic protection effect of the combined sand barrier is poor.

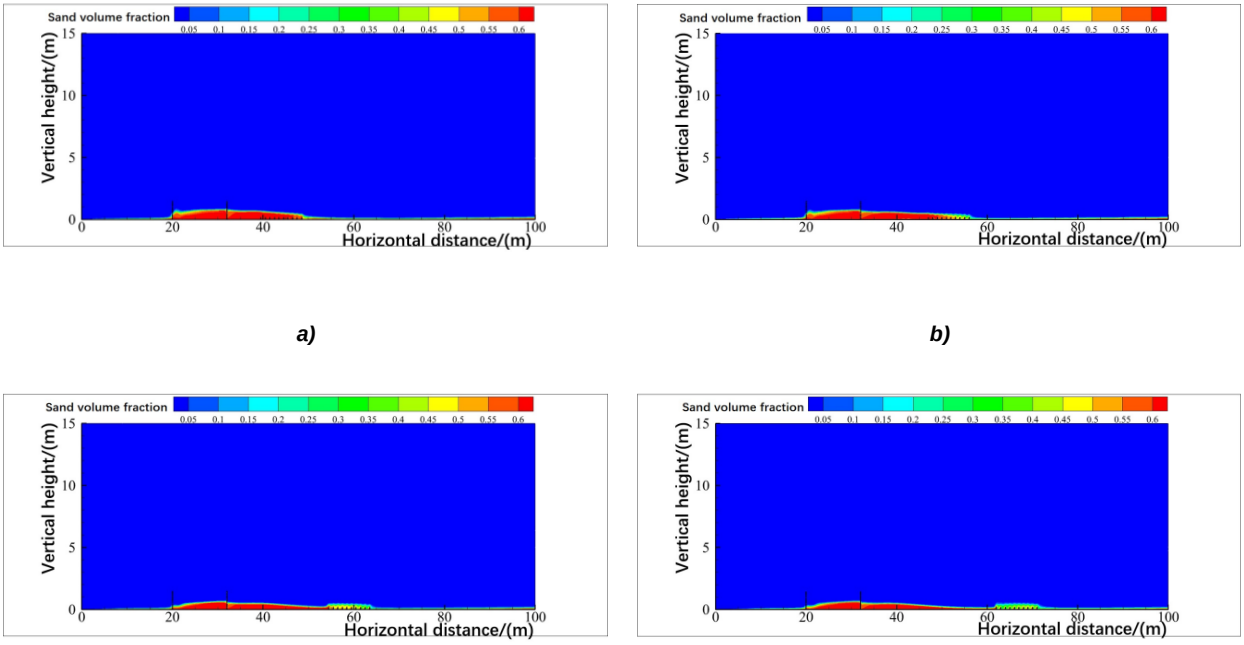

Fig. 11 – Cloud map of sand accumulation around the joint sand barrier
a) D=5H; b) D=10H; c) D=15H; d) D=20H.

The results and analysis of the wind tunnel experiment

The distribution characteristics of sand accumulation in the wind tunnel test are shown in Figure 12. It can be found that the high vertical sand barrier plays a full role in preventing sand, and a large number of sand particles are deposited near the high vertical sand barrier. As the distance between the grass grid sand barrier and the high vertical sand barrier increases, the proportion of the area covered by sand accumulation between the second sand barrier and the grass grid gradually decreases, and the sand accumulation in the grass grid gradually decreases. However, the accumulation of sand near the high vertical sand barrier has mostly stayed the same. The sediment distribution characteristics of the wind tunnel test under four conditions are basically consistent with the numerical simulation results, which verifies the reliability of the numerical simulation results.

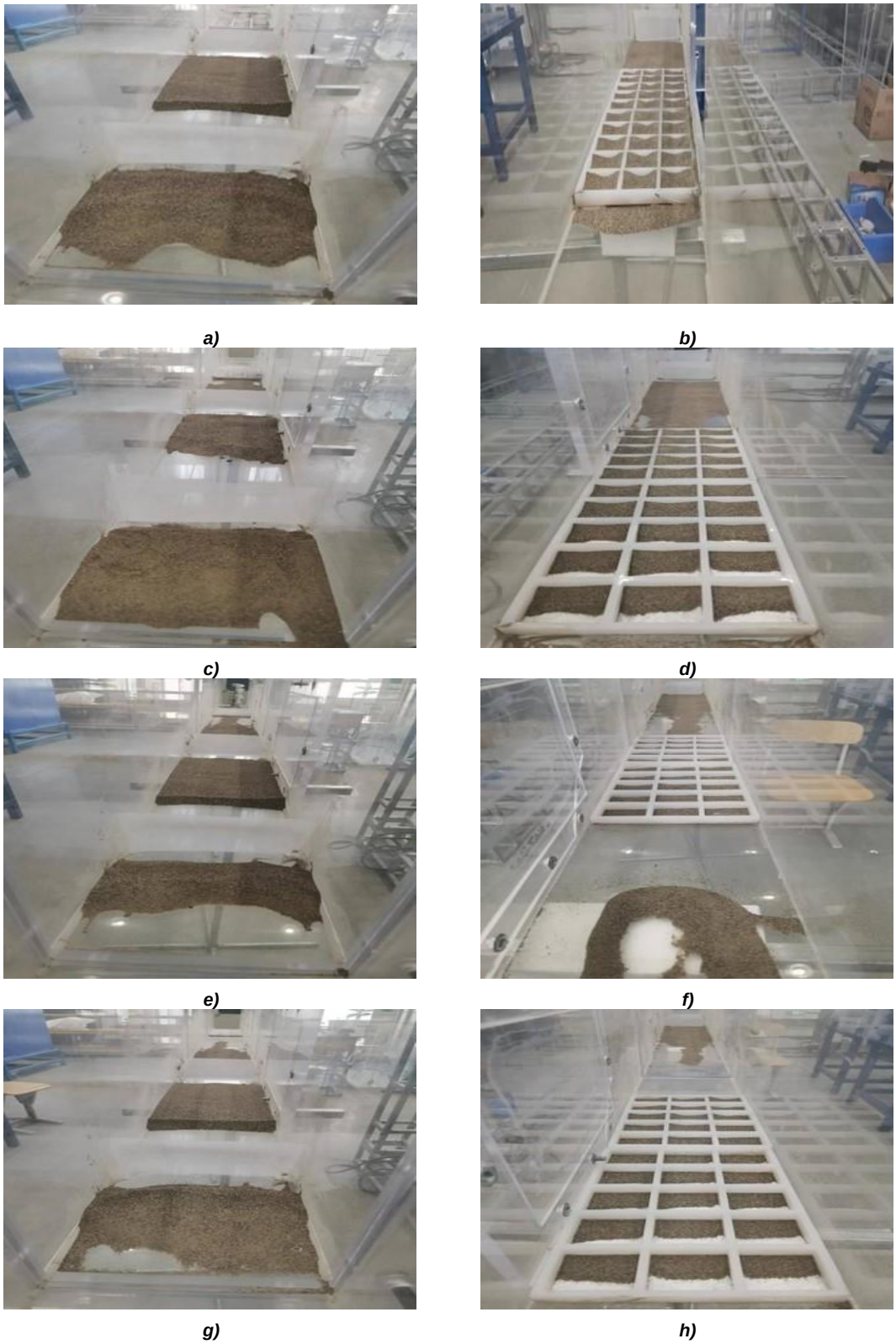

Fig. 12 – The distribution of sand accumulation in joint sand barriers at different spacings:
a) D=5H; b) D=5H; c) D=10H; d) D=10H; e) D=15H; f) D=15H; g) D=20H; h) D=20H.

After about 50 min of continuous sand blowing at 7 m/s for the joint sand barrier model with different spacing distributions, the amount of sand coming from the cavity collected by the sand collecting instrument and the amount of sand coming from the combined sand barrier placed (3H on the lee side) were drawn as a bar chart, as shown in Figure 13. It can be found that with the increase of the distance between the grass grid sand barrier and the high vertical sand barrier, the amount of sediment intercepted by the combined sand barrier gradually increases, but when D=15H, the amount of sediment accumulated by the sand collecting instrument behind the combined sand barrier increases sharply. It shows that when D=5H and 10H, the combined sand barrier can cut more sand, and the protection efficiency is better.

In order to quantify the protective benefits of joint sand control measures in wind tunnel tests, the concept of sand barrier retention rate is introduced. This concept introduces itself by assuming the erosion process of ground sandy materials as a superimposed effect of pure wind shear stress and sandy wind impact abrasion *(Liu, Hou et al., 2019)*. This method can quantitatively evaluate the influence of sand barriers on particle retention of sand material. That is, when the eroded sand grains pass through the sand barrier, the proportion of the trapped sand grains accounts for the total sand grains. The specific formula is as follows:

$$n=\frac{W\text{-}Q}{W}\times 100\% \tag{10}$$

In this equation: n is the retention rate of the sand barrier; W is the desert sediment transport flux of the same altitude layer under the same wind speed, [g/cm^2]. Q is the remaining sand transport flux after the influence of sand barrier, [g/cm^2].

By calculating, it can be found that with the increase of the spacing, the sand-blocking rate of the combined sand barrier decreases gradually. The sand-blocking rate of the combined sand barrier for 5H, 10H, 15H and 20H is 78.25%, 77.11%, 71.09% and 67.73%, respectively, indicating that the sand blocking effect of the combined sand barrier shows a decreasing trend with the increase of the spacing. By comparing the sand accumulation results of wind tunnel experiment with those of numerical simulation, it can be seen that the flow field law and sand accumulation distribution law obtained by numerical calculation and analysis are similar to the variation trend of sand accumulation law measured by wind tunnel test. And there is a corresponding relationship, which further confirms the correctness of the numerical calculation results.

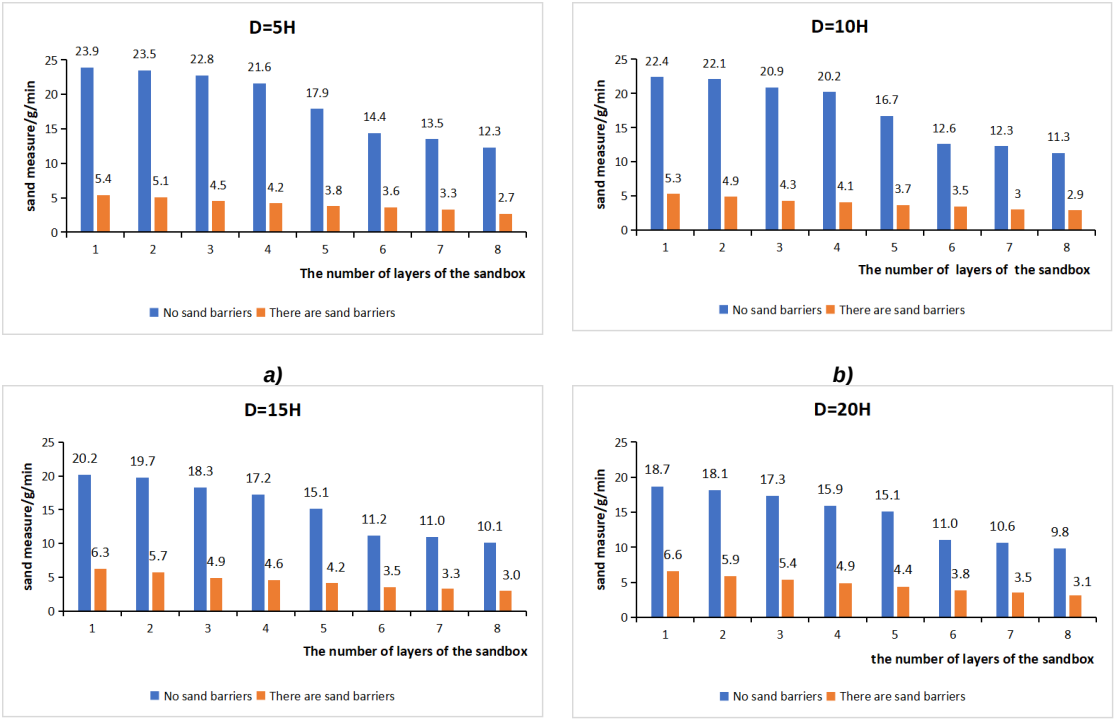

Fig. 13 – Sand trapping capacity of joint sand barriers at different spacings:
a) D=5H; b) D=10H; c) D=15H; d) D=20H.

CONCLUSION

In this study, the wind-sand flow field characteristics and protection effect around the double-row nylon mesh high vertical sand barriers and grass square joint sand barriers under extreme wind-sand environment were analyzed by Fluent numerical simulation. Then the wind tunnel test was used to verify the numerical simulation results, and the following conclusions were drawn.

1. When the distance between the double-row vertical sand barrier and the grass grid was 5H and 10H, the airflow velocity behind the double-row vertical sand barrier could not fully develop, and the low-speed area behind the double-row vertical sand barrier was basically covered with grass grid; when the spacing between the double-row vertical sand barrier and the grass grid was 15H and 20H, the airflow behind the double-row vertical sand barrier produced a certain speed recovery zone, and the airflow low-speed zone could not cover the grass grid;

2. When the spacing was 5H and 10H, the average windproof efficiency of the combined sand barrier reached more than 85%, and the effective protection distance completely covered the entire combined sand barrier area. When the spacing continued to increase, the average windproof efficiency decreased to less than 80%, and the effective protection distance could not cover the grass grid sand barrier;

3. When the spacing was 5H and 10H, the increase of airflow velocity behind the second vertical sand barrier was slight, and a large number of near-surface sand particles were fixed in the grass grid, then the sand resistance rate was over 70%, and the combined sand barrier had a good synergistic protection effect. As the distance continued to increase, the air velocity behind the second high vertical sand barrier gradually increased, even more than the sand-driving wind speed. The airflow carried most of the near-sand particles up and continued to move backward, and the sand accumulation in the grass grid was very slight. So, the sand resistance rate decreased and the synergistic protection effect of the combined sand barrier was poor.

In order to better protect the agricultural and ecological restoration areas at the edge of the desert in the Minqin area of China from wind and sand, it is recommended that the spacing between the double-row high-standing sand barriers and the grass checkered sand barrier should be 5H to 10H. Meanwhile, many farmlands, ecological restoration areas, and other agricultural areas around the desert in Northwest China are affected by strong sandstorms all year round, resulting in a decline in agricultural yield, low plant survival rate, and huge economic losses. It is hoped that this study can provide some theoretical and technical support for the design of sand control projects in farmland and ecological restoration areas in the desert areas of Northwest China.

ACKNOWLEDGMENTS

The authors were funded for this project by the National Natural Sciences Foundation of China (NSFC), Grant/Award Number: 12362033.

REFERENCES

[1] Chang L., Hailong W., Jing S. (2023). Research on the optimization of design parameters for comprehensive windbreak and sand fixation systems (综合防风固沙体系设计参数优化研究). *Journal of The China Railway Society*, Vol. 42, pp. 135-144. Beijing/China.

[2] Cuicui J., Xuemei Y., Fang C., et al. (2021). Spatio-temporal evolution of photosynthetic/non-photosynthetic vegetation coverage in typical arid areas of Minqin, Gansu Province (典型干旱区甘肃民勤光合-非光合植被覆盖度时空演变分析). *Journal of Changchun Institute of Technology(Natural Science Edition)*, Vol. 22, pp. 127-135. Changchun/China.

[3] Cornelis W.M., Gabriels D. (2004). Optimal windbreak design for wind-erosion control. *Journal of Arid Environments*, Vol. 61, pp. 315-332, United States.

[4] Congmao K. (2000). Research on the Prediction and Forecasting Model of Sand Hazards in Grass (Branches) Grid Sand Barrier (草(枝条)方格沙障沙害预测预报模型的研究). *Journal of Nanchang Institute of Technology*, Vol. 02, pp. 49-59, Jiangxi/China.

[5] Dong G., Chen T., Ren C., et al. (2023). Wind tunnel investigation of wind reduction effect under porous fences protection. *Journal of Wind Engineering and Industrial Aerodynamics*, Vol. 02, pp. 232, United States.

[6] Dong Z., Chen G., He X., et al. (2002). Controlling blown sand along the highway crossing the Taklimakan Desert. *Journal of Arid Environments*, Vol. 57, pp. 329-344, United States.

[7] Fang H., Wu X., Zou X., et al. (2018). An integrated simulation-assessment study for optimizing wind barrier design. *Agricultural and Forest Meteorology*, Vol. 263, pp. 198-206, United States.

[8] Fugui H., Ming Z., Fengzhao C., et al. (2009) Characteristics of sand and dust weather and its influencing factors in the Shazhou area of Minqin County over the past 50 years (民勤沙区 50 多年来沙尘天气特征及其影响因素). *Arid Zone Research | Arid Zone Res*, Vol. 26, pp. 889-894. Wulumuqi/China.

[9] Guowei X., Ning H., Jie Z., et al. (2021). Investigations into the design of sand control fence for Gobi buildings. *Aeolian Research*, Vol. 49, pp. 100662, United States.

[10] Guangpu J., Hejun Z., Haibing W., et al. (2020). Numerical simulation and experiment of wind and sand movement characteristics around high vertical nylon mesh sand barriers (高立式尼龙网沙障周围风沙运动特性的数值模拟与试验). *Transactions of the Chinese Society of Agricultural Engineering*, Vol. 36, pp. 109-117, Beijing/China.

[11] Guoping Z., Hejun Z., Lianxiu X., et al. (2008). Study on the windbreak and sand blocking benefits of sand willow barriers (沙柳沙障防风阻沙效益的研究). *Journal of Soil and Water Conservation*, Vol. 02, pp. 38-42, Beijing/China.

[12] Jia Y., Xiang Y. (2019). Application of Grass Square Grid Sand Barrier in Wind Prevention and Sand Fixation (草方格沙障在防风固沙中的应用). *Construction & Design for Project*, Vol. 21, pp. 205-207, Beijing/China.

[13] Jianjun Q. L., et al. (2002). Research on the Sand Control Effect of Nylon Mesh Fence (尼龙网栅栏防沙效应研究). *Journal of Lanzhou University*, Vol. 02, pp. 171-176. Lanzhou/China.

[14] Jianjun Q. L., et al. (2001). Wind tunnel simulation experiment on sand prevention effect of nylon mesh fence (尼龙网栅栏防沙效应的风洞模拟实验). *Journal of Desert Research*, Vol. 21, pp. 276-280, Lanzhou/China.

[15] Jiguo Z. (1987). Change of surface morphology after shifting sand control in Shapotou area, southeast edge of Tengger Desert (腾格里沙漠东南缘沙坡头地区流沙治理后地表形态变化). *Journal of Desert Research*, Vol. 1, pp. 12-20, Lanzhou/China.

[16] Jun L., Renhua W. (1982). Discussion on the width of semi concealed wheat straw grid sand barrier protection belt (半隐蔽式麦草方格沙障防护带宽度的探讨). *Journal of Desert Research*, Vol. 2, pp. 20-27, Lanzhou/China.

[17] Liu H., Hou Z., Chen Z., et al. (2019). Effects of standing stubble on the interception of soil erosion particles. *Land Degradation & Development*, Vol. 30, pp. 328-336, United States.

[18] Mao L., Ling S., Jie L., et al. (2024). Wind tunnel experiment on windproof effect of double row nylon sand blocking net grass grid combined sand barrier (双排尼龙阻沙网-草方格联合沙障防风效应的风洞实验). *Journal of Desert Research*, Vol. 44, pp. 9-17, Lanzhou/China.

[19] Ming W. (2007). *Large-eddy Simulation of Three Dimensional Turbulent Aeolian Motion and Numerical Simulation of Evolution of Sand Ripples* (三维湍流风沙运动的大涡模拟及沙漠地貌的数值模拟). Master's dissertation. Hohai university, Nanjing.

[20] Peng H., Jin A., Zhang S., et al. (2023). Numerical Simulation and Parameter Optimization of a New Reed–Nylon Net Combined Sand Fence. *Sustainability*, 15(18). Vol. 15, pp. 13920, United States.

[21] Papesch A.J.G. (1992). Wind tunnel test to optimize barrier spacing and porosity to reduce wind damage in horticultural shelter systems. *Journal of Wind Engineering and Industrial Aerodynamics*, Vol. 44, pp. 2631-2642, United States.

[22] Qiu G.Y., Lee I-B, Shimizu H., et al. (2004). Principles of sand dune fixation with straw checkerboard technology and its effects on the environment. *Journal of Arid Environments*, Vol. 56, pp. 449-464, United States.

[23] Tao W., Jianjun Q., Yuquan L., et al. Wind tunnel test on the effect of metal net fences on sand flux in a Gobi Desert. *Journal of Arid Land*, Vol. 9, pp. 888-889, United States.

[24] Tao W., Jianjun Q., Yuquan L., et al. (2017). Shelter effect efficacy of sand fences: A comparison of systems in a wind tunnel. *Aeolian Research*, Vol. 30, pp. 32-40, United States.

[25] Wu X., Zou X., Zhang C., et al. (2013). The effect of wind barriers on airflow in a wind tunnel. *Journal of Arid Environments*, Vol. 97, pp. 73-83, United States.

[26] Xin G., Zhang J., Fan L., et al. (2023). Numerical Simulations and Wind Tunnel Experiments to Optimize the Parameters of the Second Sand Fence and Prevent Sand Accumulation on the Subgrade of a Desert Railway. *Sustainability*, Vol. 15, pp. 12761, United States.

[27] Xu B., Zhang J., Huang N., et al. (2018). Characteristics of Turbulent Aeolian Sand Movement Over Straw Checkerboard Barriers and Formation Mechanisms of Their Internal Erosion Form. *Journal of Geophysical Research: Atmospheres*, Vol. 123, pp. 6907-6919, United States.

[28] Xiao J. (2016). *The Numerical Simulation Research on Response Rules of Wind-Blown Sand Two Phase Flow to Railway Embankment and the Wind-break Retaining Sand Wall* (风沙两相流对铁路路堤及防风沙墙响应规律的数值模拟研究). Master's dissertation. Lanzhou Jiaotong University, Lanzhou.

[29] Xianpan X. (2015). *numerical simulation of dispersion characteristics of sand particles in straw checkerboard barriers* (沙粒在草方格沙障内弥散特征的数值模拟). Master's dissertation, Lanzhou university, Lanzhou.

[30] Xunming W., Zhiwen H., Zhibao D. (1999). The Benefit of the Prevention System along the Desert Highway in Tarim Basin (塔里木沙漠公路沿线机械防沙体系效益分析). *Journal of Desert Research*, Vol. 19, pp. 120-127. Lanzhou/China.

[31] Xunming W. (1997). Benefit evaluation of mechanical sand prevention system along Tarim Desert Highway and preliminary exploration of reasonable width of sand prevention belt (塔里木沙漠公路沿线机械防沙体系效益评价及防沙带合理宽度的初步探讨). *Journal of Arid Land Resources and Environment*, Vol. 11, pp. 29-36, Neimeng/China.

[32] Yanli Z. (2011). *Research on Ecological Security Synthetic Assessment of Minqin* (民勤县生态安全综合评价研究). Master's dissertation, Beijing Agricultural University, Beijing.

[33] Yingxin L. (1987). Establishment and Benefits of Sand Prevention System for Shapotou Section of Baolan Railway (包兰铁路沙坡头地段铁路防沙体系的建立及其效益). *Journal of Desert Research*, Vol. 7, pp. 1-11, Lanzhou/China.

[34] Zhang C., Li Q., Zhou N., et al. (2016). Field observations of wind profiles and sand fluxes above the windward slope of a sand dune before and after the establishment of semi-buried straw checkerboard barriers. *Aeolian Research*, Vol. 20, pp. 59-70, United States.

[35] Zheng H. (2006). *Study of new sand-fixing materials and the field integrated sand-fixing technology* (固沙用新材料及野外固沙综合技术研究). Master's dissertation. Lanzhou university, Lanzhou.

[36] Zhengyi Y., Guangting C., Zhiwen H., et al. (2006). The decline process of sand prevention function of mechanical sand prevention system (机械防沙体系防沙功能的衰退过程). *Journal of Desert Research*, Vol. 26, pp. 226-231, Lanzhou/China.

[37] Zhibao D.Z. (2005). Research Achievements in Aeolian Physics in China for Last Five Decades(Ⅱ) (中国风沙物理研究 50a(Ⅱ)). *Journal of Desert Research*, Vol. 25, pp. 795-815. Lanzhou/China.

[38] Zhenting W. (2002). A simple model for size analysis of grass square grid sand barrier (草方格沙障尺寸分析的简单模型). *Journal of Desert Research*, Vol. 22, pp. 229-232. Lanzhou/China.